actuators

MDPI

*Article*

# Incremental Sliding Mode Control for Predefined-Time Stability of a Fixed-Wing Electric Vertical Takeoff and Landing Vehicle Attitude Control System

**Jujiang Liu [1,2,*] and Yusong Tan [1]**

[1] College of Computer, National University of Defense Technology, Changsha 410073, China; ystan@nudt.edu.cn
[2] Automotive Engineering Research Institute, Guangzhou Automobile Group Co., Ltd., Guangzhou 511434, China
* Correspondence: liujj@gacrnd.com

**Abstract:** This paper presents a novel incremental sliding mode control scheme to address the attitude-tracking issue in both the helicopter and airplane modes of an electric vertical takeoff and landing vehicle, guaranteeing the stabilization of the attitude-tracking error within a predefined time. Firstly, an incremental model of the vehicle's attitude control system with external disturbances is established. The high-order terms of the incremental model and instantaneous perturbations are retained as lumped terms rather than directly discarding them to ensure the accuracy of the incremental model. Then, a novel nonsingular sliding surface is developed. Once the ideal sliding motion is established, the states on the sliding surface will converge to the equilibrium point within a predefined time. Furthermore, a predefined-time incremental sliding mode controller is developed by using sliding mode control and incremental control techniques. It effectively reduces the reliance on the model information and attenuates the effects of external disturbances. The predefined-time stability of the entire controlled system is rigorously proven using Lyapunov theory. Finally, numerical simulation examples verify the effectiveness of the proposed control scheme.

**Keywords:** urban air mobility; electric vertical takeoff and landing vehicle; sliding mode control; incremental control; predetermined-time stability

check for updates

**Citation:** Liu, J.; Tan, Y. Incremental Sliding Mode Control for Predefined-Time Stability of a Fixed-Wing Electric Vertical Takeoff and Landing Vehicle Attitude Control System . *Actuators* **2024**, *13*, 371. https://doi.org/10.3390/act13090371

Academic Editor: Han Sol Kim

Received: 27 August 2024
Revised: 14 September 2024
Accepted: 19 September 2024
Published: 20 September 2024

**Copyright:** © 2024 by the authors. Licensee MDPI, Basel, Switzerland. This article is an open access article distributed under the terms and conditions of the Creative Commons Attribution (CC BY) license (https://creativecommons.org/licenses/by/4.0/).

## 1. Introduction

Urban air mobility (UAM) is a new concept that has emerged in recent years, regarded as a safe, efficient, and sustainable mode of transportation that can reduce congestion and improve the quality of life for urban and suburban residents. It is seen as an efficient and sustainable new mode of transportation for the future. Industry, academia, and authoritative institutions like NASA, Uber, Airbus, Boeing, Joby Aviation, E-Hang, etc., are conducting research on essential technologies to make UAM a reality, driven by the tremendous prospects it offers [1]. Therefore, developing a revolutionary transportation vehicle is the most important component. The compound-wing electric vertical takeoff and landing (eVTOL) vehicle features advanced hovering systems with multiple rotors and high-lift wing bodies with fixed wing configurations [2]. It can take off and land vertically, reducing the need for traditional airport infrastructure, and it can also cruise efficiently with aerodynamic lift. eVTOL vehicles meet the UAM's on-demand point-to-point transportation needs. It has received increasing attention in recent years [3,4]. Different layout configurations distinguish these eVTOL vehicles into four main types: multi-rotor eVTOL vehicles, compound-wing eVTOL vehicles, tilt-rotor (wing) eVTOL vehicles, and tail-mounted eVTOL vehicles. Among them, the compound-wing eVTOL vehicle configuration improves flight speed and endurance, expanding the flight envelope, thereby garnering extensive research [5–11].

The eVTOL vehicle is a highly nonlinear system whose control performance is easily affected by external aerodynamics, unmodeled disturbances, and parameter uncertainties. Therefore, researchers have proposed various nonlinear flight control schemes for eVTOL vehicles. The active disturbance rejection control method was employed in tiltrotor transition control and realized a fast mode transition from level flight to hovering in [12,13]. A nonlinear observer-based backstepping control law was developed in the takeoff, hovering, and landing phases of an eVTOL vehicle with external disturbances [14]. A robust full-envelope control scheme was developed for eVTOL vehicles in [15] by the H∞ methods. With the development of intelligent control technology, the deep reinforcement learning method was also adopted in the eVTOL vehicle's mobility control, but the model uses three degrees of freedom, where attitude stability is not considered [16]. Moreover, nonlinear dynamic inversion (NDI) is a well-known nonlinear control technique that has been widely used in a variety of plants [17–19]. A control architecture within the framework of NDI was proposed to accomplish a full envelope flight mission for an eVTOL vehicle model in [19], but with a focus only on its longitudinal motion to demonstrate the effectiveness of the approach. A unified framework was suggested that combines an NDI controller with a flight mode switching method for the full envelope control of a quadrotor eVTOL vehicle, including cruise-speed flight, low-speed hover, and the transition between these flight regimes [20].

However, the aforementioned control methods must know exactly the system's model information for the stability proof of the closed-loop control system. Meeting this criterion in practice is difficult due to the modeling simplification and the existing external disturbances. A sensor-based control methodology known as incremental nonlinear dynamic inversion (INDI) improves the system's robustness against model uncertainty by reducing the use of model information [21–23].

The flight control system was then synthesized using INDI techniques in [2,24], the attitude angle control loop for a compound-wing eVTOL vehicle relied on classic NDI, while the attitude angle rate control loop relied on INDI, which employed an extended state observer to estimate the angular acceleration, thereby ensuring the robustness, safety, and smoothness of the transition phase for the eVTOL vehicle. In [25], INDI was used for integrated attitude/altitude control of a quad tiltrotor eVTOL vehicle for hover, low forward speed, and attitude control. The weighted least squares control allocation algorithm was integrated into the altitude controller to address thrust saturation constraints. An INDI controller integrating an optimization-based control allocation method was developed in [26] to address the challenge of flight control with significant nonlinearity, resulting in a unified flight controller that covers a wide flight envelope. Considering the over-actuated characteristics of eVTOL systems [27], an incremental nonlinear control allocation method based on its incremental control allocation model was proposed, which can optimally allocate control commands to a set of available control actuators to enable redundant actuators to play a role in maneuverability and efficiency. However, these closed-loop control systems with INDI controllers can only achieve asymptotic stability. To improve the control system's convergence speed, an incremental adaptive sliding mode control scheme was proposed in [28] to address an eVTOL vehicle's fault-tolerant control problem, with the whole controlled system's finite-time convergence guaranteed in the Lyapunov sense. A finite-time convergence INDI controller combined with a control allocation technique was implemented in a wing aircraft's inner angular rate loop [29]. A finite-time disturbance observer-based incremental backstepping attitude controller was devised to improve the robustness of the standard backstepping controller [30]. However, the convergence time upper bound is related to the system's initial state value.

Motivated by the aforementioned fact, this paper suggests a new incremental sliding mode attitude control scheme for an eVTOL vehicle with external disturbances. It ensures that the required attitude signal can be accurately followed within a predefined time. The main contributions can be stated as follows: (1) An incremental model of the eVTOL vehicle attitude control system with external disturbances is first established and the Taylor

high-order terms are lumped as a synthetic term. Compared with the conventional incremental control methods [21,22,31–33], this paper does not omit the higher-order term, although the high sampling frequency assumption existed. It is beneficial for reducing the dependence of the devised controller on the model information. (2) Using the sliding mode control technique and the Lyapunov-based predefined-time control approach, a novel non-singular predefined-time sliding mode surface is developed for the attitude control system. Once the ideal sliding motion is established, the state's convergence time to the equilibrium is predefined. (3) With the application of the sliding mode control and incremental control techniques, a predefined-time incremental controller synthesizing a robust control command is proposed. It is active in attenuating disturbances and reduces the computational complexity by using the established incremental system model. The Lyapunov method provides rigorous proofs that, when compared with these finite-time control methods [28–30], the proposed control scheme can ensure the closed-loop system achieve predefined-time stability. Simulation simulation results provide a comprehensive exposition of the proposed controller's behavior, including its control accuracy and settling time.

The subsequent sections of this paper are organized as follows: The preliminaries and modeling are provided in Section 2. Section 3 presents a predefined-time incremental sliding mode controller design method. The numerical simulation examples are conducted to validate the effectiveness of the proposed control method in Section 4. Finally, Section 5 summaries this paper.

## 2. Materials and Modeling

### *2.1. The Target eVTOL Vehicle*

As shown in Figure 1 (Adapted from Ref. [2]), a simplified model of the target eVTOL vehicle, VtolA7, studied in this paper is presented, which is a compound-wing fixed-wing unmanned aerial vehicle with eVTOL characteristics. Its physical parameters are listed in Table 1. As a compound-wing eVTOL vehicle, VtolA7 has both four evenly distributed rotors (they provide lift $T_1$, $T_2$, $T_3$, and $T_4$, respectively) and traditional fixed-wing aircraft actuators, including ailerons ($\delta_a$), elevators ($\delta_e$), rudders ($\delta_r$), and front propellers (thrust $T_5$). As a result, the compound-wing VtolA7 has both a hovering power system and a propulsion power system. Four evenly distributed rotors on the wings provide the hovering system with upward lift, while a horizontally installed rotor in front of the cabin powers the propulsion system during cruising flight. It can be used as a test eVTOL vehicle for verifying the control scheme as well as a key vehicle for future UAM.

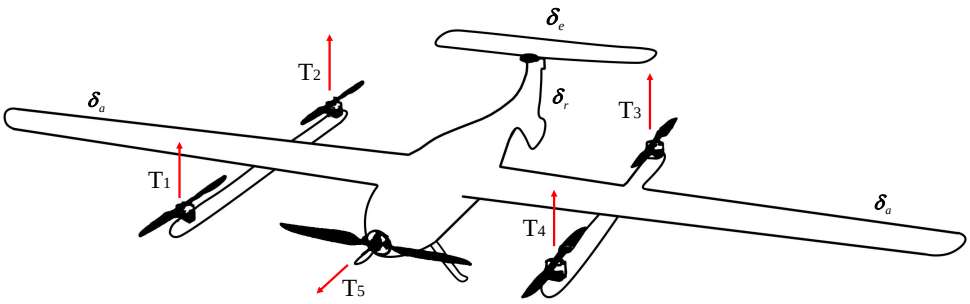



**Figure 1.** Overview of the target eVTOL unmanned aerial vehicle VtolA7.

The complete flight envelope of an eVTOL vehicle includes vertical takeoff, hover, transition to forward flight, cruise, climb/descend and turn, transition to hover, and vertical landing. When the eVTOL vehicle's airspeed is low, the aerodynamic control surface's insufficient control efficiency fails to counterbalance the thrust displacement-induced pitch moment. The rotor system and thrust system jointly control the airspeed to prevent sudden changes in altitude and attitude, thereby achieving stable acceleration from zero airspeed to cruise speed. With the continuous increase in airspeed, the wing body's aerodynamics

become more dominant, allowing the aerodynamic control surface to partially balance the propulsion system's pitch moment. The rotor system cuts off when the airspeed approaches the cruising airspeed, allowing the propulsion system to independently control the airspeed. Aerodynamics fully achieves attitude control when the eVTOL vehicle is in a fixed-wing mode during cruise.

**Table 1.** Physical parameters the target eVTOL.

| Variable | Explanation | Value |
|---|---|---|
| $S$ | Reference area | 0.460 $m^2$ |
| $b$ | Wingspan | 2.286 m |
| $c$ | Mean aerodynamic chord | 0.2 m |
| $m$ | Mass | 6.2 Kg |
| $I_x$ | Moment of inertia around the $x$- axis | 0.5614 Kg·$m^2$ |
| $I_y$ | Moment of inertia around the $y$-axis | 0.4479 Kg·$m^2$ |
| $I_z$ | Moment of inertia around the $z$-axis | 0.8700 Kg·$m^2$ |

### *2.2. The Mathematical Model of the eVTOL*

The overview of the eVTOL vehicle is shown in Figure 1. Let $\boldsymbol{\Theta} = [\phi \ \ \theta \ \ \psi]^\top \in \mathbb{R}^3$ being the Euler angle vector (roll, pitch, and yaw) of the eVTOL vehicle and $\boldsymbol{\chi} = [x \ \ y \ \ h]^\top \in \mathbb{R}^3$ being the position vector of the eVTOL vehicle regarding the earth reference (inertial) frame. $h = -z$ denotes the altitude of the eVTOL vehicle. Therefore, the kinematic models are represented as

$$\begin{bmatrix} \dot{\phi} \\ \dot{\theta} \\ \dot{\psi} \end{bmatrix} = \begin{bmatrix} 1 & \sin\phi\tan\theta & \cos\phi\tan\theta \\ 0 & \cos\phi & -\sin\theta \\ 0 & \sin\phi\sec\theta & \cos\phi\sec\theta \end{bmatrix} \begin{bmatrix} p \\ q \\ r \end{bmatrix} \tag{1}$$

$$\begin{bmatrix} \dot{x} \\ \dot{y} \\ \dot{z} \end{bmatrix} = \begin{bmatrix} \cos\theta\cos\psi & \sin\phi\sin\theta\cos\psi - \cos\phi\sin\psi & \cos\phi\sin\theta\cos\psi + \sin\phi\sin\psi \\ \cos\theta\sin\psi & \sin\phi\sin\theta\sin\psi + \cos\phi\cos\psi & \cos\phi\sin\theta\sin\psi - \sin\phi\cos\psi \\ -\sin\theta & \sin\phi\cos\theta & \cos\phi\cos\theta \end{bmatrix} \begin{bmatrix} u \\ v \\ w \end{bmatrix} \tag{2}$$

where $\boldsymbol{V} = [u \ \ v \ \ w]^\top \in \mathbb{R}^3$ and $\boldsymbol{\omega} = [p \ \ q \ \ r]^\top \in \mathbb{R}^3$ denote the velocity vector and the angular rate vector. It is well known that the dynamics equations of the eVTOL vehicle can be expressed in the standard form as [2,14]

$$\dot{\boldsymbol{V}} = \frac{1}{m}\left(\boldsymbol{F}_{\text{total}} - \boldsymbol{\omega}^{\times} m\boldsymbol{V}\right) + \boldsymbol{d}_v \tag{3}$$

$$\dot{\boldsymbol{\omega}} = \boldsymbol{I}^{-1}\left(\boldsymbol{M}_{\text{total}} - \boldsymbol{\omega}^{\times}\boldsymbol{I}\boldsymbol{\omega}\right) + \boldsymbol{d}_\omega \tag{4}$$

with $\boldsymbol{I} \in \mathbb{R}^{3\times3}$ being the inertia matrix. $\boldsymbol{d}_v \in \mathbb{R}^3$ and $\boldsymbol{d}_\omega \in \mathbb{R}^3$, respectively, represent the comprehensive disturbance force and disturbance torque, mainly a blend of state measurement deviation and model parameter uncertainty. The disturbances from the external environment are transformed into the internal uncertainty of the model, as the impact of external disturbances is mainly due to changes in the flow angle, resulting in changes in the aerodynamic characteristics of the vehicle. The total force $\boldsymbol{F}_{\text{total}} = [X_{\text{total}} \ \ Y_{\text{total}} \ \ Z_{\text{total}}]^\top \in \mathbb{R}^3$ and moment $\boldsymbol{M}_{\text{total}} = [L_{\text{total}} \ \ M_{\text{total}} \ \ N_{\text{total}}]^\top \in \mathbb{R}^3$ are composed of contributions from aerodynamics, propulsion, and gravity. They are computed by

$$\mathbf{F}_{\text{total}} = \mathbf{F}_{\text{aero}} + \mathbf{F}_{\text{prop}} + \mathbf{F}_{\text{grav}} \tag{5}$$

$$\mathbf{M}_{\text{total}} = \mathbf{M}_{\text{aero}} + \mathbf{M}_{\text{prop}} \tag{6}$$

where the subscripts aero, prop, and grav represent abbreviations for aerodynamics, propulsion, and gravity, respectively. What follows is an explanation of the aerodynamic contribution using the dimensionless coefficients

$$\mathbf{F}_{\text{aero}} = \begin{bmatrix} C_X \\ C_Y \\ C_Z \end{bmatrix} \bar{q}S, \quad \mathbf{M}_{\text{aero}} = \begin{bmatrix} bC_l \\ \bar{c}C_m \\ bC_n \end{bmatrix} \bar{q}S \tag{7}$$

with the dimensionless aerodynamic coefficients being a combination of conventional lift, drag, and lateral force coefficients and corresponding plate coefficients. $S$ is the wing area and $\bar{q}$ denotes dynamic pressure. Additionally, the aerodynamic coefficients must be converted from the aerodynamic reference frame to the vehicle's own reference frame when the eVTOL vehicle flies at high airspeed.

$$\begin{bmatrix} C_X \\ C_Y \\ C_Z \end{bmatrix} = \begin{bmatrix} \cos\alpha & 0 & -\sin\alpha \\ 0 & 1 & 0 \\ \sin\alpha & 0 & \cos\alpha \end{bmatrix} \begin{bmatrix} \cos\beta & -\sin\beta & 0 \\ \sin\beta & \cos\beta & 0 \\ 0 & 0 & 1 \end{bmatrix} \begin{bmatrix} -C_D \\ -C_Y \\ -C_L \end{bmatrix} \tag{8}$$

$$\begin{bmatrix} C_D \\ C_Y \\ C_L \end{bmatrix} = (1-\eta) \begin{bmatrix} C_D \\ C_Y \\ C_L \end{bmatrix}_{\text{aero}} + \eta \begin{bmatrix} C_p \sin\alpha\cos\beta \\ C_p \sin\beta \\ C_p \sin\alpha\cos\alpha \end{bmatrix} \tag{9}$$

where $\alpha$ and $\beta$ represent the angle of attack and sideslip angle derived from the eVTOL vehicle's attitude control system. $\eta$ is the mixing coefficient of the eVTOL vehicle between hovering and forward flight, gradually changing between 0 and 1 during the transition phase, and vice versa. This coefficient's magnitude is dependent on airspeed. In the fully hovering state, $\eta$ is 1, and in the pure forward flight state, it is 0. Equation (8) is based on traditional aerodynamic modeling of a flat plate, where $C_p = 2$ [25]. Similarly, we apply the mixing coefficient to aerodynamic torque, anticipating that the plate effect will not affect the dimensionless aerodynamic torque coefficient.

$$\begin{bmatrix} C_l \\ C_m \\ C_n \end{bmatrix} = (1-\eta) \begin{bmatrix} C_l \\ C_m \\ C_n \end{bmatrix}_{\text{aero}} \tag{10}$$

The dimensionless aerodynamic moment coefficients depend both on the relevant aerodynamic states as well as the aerodynamic control effectors (control surfaces), as follows

$$\begin{bmatrix} C_l \\ C_m \\ C_n \end{bmatrix}_{\text{aero}} = \begin{bmatrix} C_l(\beta,p,r) \\ C_m(\alpha,q,\delta_{\text{fl}}) \\ C_n(\beta,p,r) \end{bmatrix} + \begin{bmatrix} C_{l_{\delta_\text{a}}} & 0 & C_{l_{\delta_\text{r}}} \\ 0 & C_{m_{\delta_\text{e}}} & 0 \\ C_{n_{\delta_\text{a}}} & 0 & C_{n_{\delta_\text{r}}} \end{bmatrix} \begin{bmatrix} \delta_\text{a} \\ \delta_\text{e} \\ \delta_\text{r} \end{bmatrix} \tag{11}$$

with the control effectors of the eVTOL vehicle being aileron, elevator, and rudder deflection angle $\delta_j$ with $j = a, e, r$. $C_l(\beta,p,r)$, $C_m(\alpha,q,\delta_{\text{fl}})$, and $C_n(\beta,p,r)$ denote the torque coefficients independent of each rudder angles $\delta_\text{a}$, $\delta_\text{e}$, and $\delta_\text{r}$. $C_{l_{\delta_\text{a}}}$, $C_{l_{\delta_\text{r}}}$, $C_{m_{\delta_\text{e}}}$, $C_{n_{\delta_\text{a}}}$, and $C_{n_{\delta_\text{r}}}$ are nominal aerodynamic coefficient of the eVTOL vehicle. The gravity contribution is expressed as

$$\mathbf{F}_{\text{grav}} = \begin{bmatrix} X_{\text{grav}} \\ Y_{\text{grav}} \\ Z_{\text{grav}} \end{bmatrix} = \begin{bmatrix} -\sin\theta \\ \sin\phi\cos\theta \\ \cos\phi\cos\theta \end{bmatrix} mg \tag{12}$$

Furthermore, the propulsion contributions are given by

$$\mathbf{F}_{\text{prop}} = \begin{bmatrix} X_{\text{prop}} \\ Y_{\text{prop}} \\ Z_{\text{prop}} \end{bmatrix} = \begin{bmatrix} T_5 \\ 0 \\ -\sum_{i=1}^{4} T_i \end{bmatrix} \tag{13}$$

$$\mathbf{M}_{\text{prop}} = \eta \begin{bmatrix} L_{\text{prop}} \\ M_{\text{prop}} \\ N_{\text{prop}} \end{bmatrix} = \eta \begin{bmatrix} dy_f & -dy_f & dy_r & -dy_r \\ dx_f & dx_f & -dx_r & -dx_r \\ k_m & -k_m & -k_m & k_m \end{bmatrix} \begin{bmatrix} T_1 \\ T_2 \\ T_3 \\ T_4 \end{bmatrix} \tag{14}$$

with $k_m$ being the torque constant of the propellers, $(dx_f, dy_f, dz_f)$ and $(dx_r, dy_r, dz_r)$ are the locations of the front propellers and the rear propellers. $T_i$ with $i = 1, 2, 3, 4$, and 5 denote the propeller thrust, which is the control input of the hovering power system and propulsion power system.

### *2.3. The Attitude Control System of the eVTOL*

The attitude control system is crucial for an eVTOL vehicle to achieve its flight envelope. Next, we will concentrate on developing an attitude control scheme that is applicable to both rotor and fixed wing systems for the eVTOL vehicle's attitude maneuver. From (1), (4), and (6), the compact vector form of the eVTOL vehicle's attitude control system is represented as

$$\begin{cases} \dot{\boldsymbol{\Theta}} = \boldsymbol{\Gamma}(\boldsymbol{\Theta})\boldsymbol{\omega} \\ \dot{\boldsymbol{\omega}} = \boldsymbol{I}^{-1}(\mathbf{M}_{\text{total}} - \boldsymbol{\omega}^{\times}\boldsymbol{I}\boldsymbol{\omega}) + \boldsymbol{d}_{\omega} \end{cases} \tag{15}$$

The kinematic and the attitude dynamics (15) can be manipulated to obtain

$$\ddot{\boldsymbol{\Theta}} = \dot{\boldsymbol{\Gamma}}(\boldsymbol{\Theta})\boldsymbol{\omega} + \boldsymbol{\Gamma}(\boldsymbol{\Theta})(\boldsymbol{I}^{-1}(\mathbf{M}_{\text{aero}} + \mathbf{M}_{\text{prop}} - \boldsymbol{\omega}^{\times}\boldsymbol{I}\boldsymbol{\omega}) + \boldsymbol{d}_{\omega}) \tag{16}$$

Next, by introducing two new variables $\boldsymbol{x}_1 = \boldsymbol{\Theta}$ and $\boldsymbol{x}_2 = \dot{\boldsymbol{\Theta}}$, the system (16) can be written as

$$\begin{cases} \dot{\boldsymbol{x}}_1 = \boldsymbol{x}_2 \\ \dot{\boldsymbol{x}}_2 = \boldsymbol{F}(\boldsymbol{x}_1, \boldsymbol{x}_2) + \boldsymbol{G}(\boldsymbol{x}_1)(\boldsymbol{\delta} + \boldsymbol{d}_{\omega}) \end{cases} \tag{17}$$

with $\boldsymbol{F}(\boldsymbol{x}_1, \boldsymbol{x}_2) = \dot{\boldsymbol{\Gamma}}(\boldsymbol{\Theta})\boldsymbol{\omega} - \boldsymbol{G}(\boldsymbol{x}_1)\boldsymbol{\omega}^{\times}\boldsymbol{I}\boldsymbol{\omega}$, $\boldsymbol{G}(\boldsymbol{x}_1) = \boldsymbol{\Gamma}(\boldsymbol{\Theta})\boldsymbol{I}^{-1}$, and $\boldsymbol{\delta} = \mathbf{M}_{\text{aero}} + \mathbf{M}_{\text{prop}} = [L_{\text{req}} \ M_{\text{req}} \ N_{\text{req}}]^{\top} \in \mathbb{R}^3$.

It should be noted that this paper primarily investigates the attitude tracking control of the eVTOL vehicle in helicopter hover mode and airplane cruise mode, without considering the flight control problem of the transition process between the two modes. That is to say, the coefficient $\eta$ can only be 1 or 0. As a result, in order to complete attitude maneuvering, we need to design an attitude controller that calculates the required control torque $\boldsymbol{\delta}$ for the eVTOL vehicle to track the desired attitude command. In fixed-wing mode, changes in the fixed-wing control surface's aerodynamics generate the required control torque. In rotor mode, the control torque is generated by the rotational speed of the four rotors.

In order for the attitude control system (17) of the eVTOL vehicle to track the desired attitude command, many nonlinear control methods have been proposed by researchers, such as adaptive control and NDI [11,17–19]. However, these methods necessitate prior knowledge of the controlled system's system term, $\boldsymbol{F}(\boldsymbol{x}_1, \boldsymbol{x}_2)$. Given the strong nonlinearity of eVTOL vehicles, the need for simplification during modeling, and the presence of external disturbances, obtaining this knowledge in real-world scenarios is challenging. Therefore, this paper aims to propose an incremental attitude control method that does not rely precisely on system model information.

### *2.4. Incremental Model of the Attitude Control System*

The first step in designing an incremental controller is to perform a first-order Taylor expansion around $\dot{\boldsymbol{x}}_{2,0}$ with the previous sampling signal of the current state for $\dot{\boldsymbol{x}}_2(t)$ in the attitude control system (17). That is to say, $\boldsymbol{x}_{2,0} = \boldsymbol{x}_2(t - \lambda)$ with $\lambda$ being the sampling

period. Therefore, the incremental dynamic model of the attitude control system can be obtained as

$$\begin{cases} \dot{\boldsymbol{x}}_1 = \boldsymbol{x}_2 \\ \dot{\boldsymbol{x}}_2 = \boldsymbol{F}(\boldsymbol{x}_{1,0}, \boldsymbol{x}_{2,0}) + \boldsymbol{G}(\boldsymbol{x}_{1,0})\boldsymbol{\delta}_0 \\ \quad + \dfrac{\partial[\boldsymbol{F}(\boldsymbol{x}_{1,0}, \boldsymbol{x}_{2,0}) + \boldsymbol{G}(\boldsymbol{x}_{1,0})\boldsymbol{\delta}_0]}{\partial \boldsymbol{x}_2}(\boldsymbol{x}_2 - \boldsymbol{x}_{2,0}) \\ \quad + \dfrac{\partial[\boldsymbol{F}(\boldsymbol{x}_{1,0}, \boldsymbol{x}_{2,0}) + \boldsymbol{G}(\boldsymbol{x}_{1,0})\boldsymbol{\delta}_0]}{\partial \boldsymbol{\delta}_0}(\boldsymbol{\delta} - \boldsymbol{\delta}_0) + \Pi\left(\Delta^2 \boldsymbol{x}_2\right) + \bar{\boldsymbol{d}}_{\omega 0} + \Delta \bar{\boldsymbol{d}}_{\omega} \end{cases} \tag{18}$$

with $\boldsymbol{\delta}_0 = \boldsymbol{\delta}(t - \lambda)$ being the previous sampling signal of the control input $\boldsymbol{\delta}$. Referring to the incremental control method, the increment of state and the control input are defined as $\Delta \boldsymbol{x}_2 = \boldsymbol{x}_2 - \boldsymbol{x}_{2,0}$ and $\Delta \boldsymbol{\delta} = \boldsymbol{\delta} - \boldsymbol{\delta}_0$, respectively. $\Pi\left(\Delta^2 \boldsymbol{x}_2\right)$ represents the aggregated higher-order terms in the Taylor expansion process. $\bar{\boldsymbol{d}}_{\omega 0}$ is the basic part of disturbances in dynamics systems, while $\Delta \bar{\boldsymbol{d}}_{\omega}$ denotes the part of state deviation caused by instantaneous changes in external disturbances. In [22], it analyzes the stability and robustness of a controlled system with external disturbances under the action of an incremental controller. In contrast, we consider the high-order terms of the Taylor expansion and the instantaneous disturbance of the incremental system to be a comprehensive term. We then introduce robust control values based on incremental control theory to enhance the system's robustness and stability, thereby achieving more rigorous theoretical outcomes.

It is reasonable to assume that for any incremental control input $\Delta \boldsymbol{\delta}$ and a sufficiently small sampling period $\lambda$, the change of $\Delta \boldsymbol{x}_2$ is minimal [34]. This means that $\Delta \boldsymbol{x}_2 \cong \boldsymbol{0}$, $\forall \Delta \boldsymbol{\delta}$. Then, the high-order term of Taylor expansion $\Pi\left(\Delta^2 \boldsymbol{x}_2\right)$ and $\Delta \bar{\boldsymbol{d}}$ are combined into a composite term $\boldsymbol{d}_1$. As a result, the incremental model (13) of the attitude control system can be rewritten as follows

$$\begin{cases} \dot{\boldsymbol{x}}_1 = \boldsymbol{x}_2 \\ \dot{\boldsymbol{x}}_2 = \dot{\boldsymbol{x}}_{2,0} + \boldsymbol{G}(\boldsymbol{x}_{2,0})\Delta \boldsymbol{\delta} + \boldsymbol{d}_1 \end{cases} \tag{19}$$

with $\dot{\boldsymbol{x}}_{2,0} = \boldsymbol{F}(\boldsymbol{x}_{1,0}, \boldsymbol{x}_{2,0}) + \boldsymbol{G}(\boldsymbol{x}_{1,0})\boldsymbol{\delta}_0 + \bar{\boldsymbol{d}}_{\omega 0}$.

Recalling the system (17), the system term $\boldsymbol{F}(\boldsymbol{x}_1, \boldsymbol{x}_2)$ disappears in the incremental system (19). This also means that incremental controllers designed based on incremental control systems can improve the robustness of the controlled system to a certain extent, as the uncertainty caused by inaccurate modeling can be eliminated. The variable $\dot{\boldsymbol{x}}_{2,0}$ represents the angular acceleration vector, which can be measured using an angular accelerometer or estimated using an observer based on other measurable states in engineering. Here, we use a second-order low-pass filter that relies solely on attitude angular velocity $\boldsymbol{x}_{2i,0}$ to accurately approximate $\dot{\boldsymbol{x}}_{2i,0}$ with $i = 1, 2, 3$ [35,36].

$$G(s) = \frac{s\varpi_n^2}{s^2 + 2\xi_n \varpi_n s + \varpi_n^2} \tag{20}$$

with $\xi_n$ and $\varpi_n$ being the appropriate damping coefficient and period coefficient, respectively.

**Assumption 1** ([35]). *Both $\Delta \bar{\boldsymbol{d}}\omega$ and $\bar{\boldsymbol{d}}_{0\omega}$ are bounded. Therefore, the lumped term $\boldsymbol{d}_1$ has an upper bound and such that $||\boldsymbol{d}_1|| \leq \gamma$ with $\gamma$ being a scalar.*

## 3. Incremental Sliding Mode Controller Design of the Attitude Control System

### *3.1. Predefined-Time Sliding Mode Surface Design*

To accomplish the attitude tracking of the eVTOL vehicle within a predefined time, define two error variables $\boldsymbol{e}_1 = \boldsymbol{x}_1 - \boldsymbol{x}_d$ and $\boldsymbol{e}_2 = \boldsymbol{x}_2 - \dot{\boldsymbol{x}}_d$. A novel nonsingular predefined-time sliding mode surface is developed as follows

$$\begin{cases} \boldsymbol{S} = \boldsymbol{e}_2 + \dfrac{\boldsymbol{e}_1 \Phi_1}{2 p_1 T_1} \\ \Phi_1 = \begin{cases} (1 + V_e^{p_1})^{\frac{3}{2}} V_e^{-p_1}, & V_e \geq \eta_1 \\ (1 + V_e^{p_1})^{\frac{3}{2}} (k_1 V_e + k_2 V_e^2), & V_e < \eta_1 \end{cases} \end{cases} \tag{21}$$

with $0 < p_1 < \frac{1}{2}$ and $V_e = \frac{1}{2}\boldsymbol{e}_1^\top \boldsymbol{e}_1$; $T_1 > 0$ is a predefined time constant; $k_1 = 2\eta_1^{-1-p_1}$ and $k_2 = -\eta_1^{-2-p_1}$ are selected to meet the continuity of $\boldsymbol{S}$. The positive real number $\eta_1$ satisfies $0 < \eta_1 < 1$. If $V_e \geq \eta_1$, the error variable $\boldsymbol{e}_1$ can converge along with the sliding mode surface $\boldsymbol{S} = 0$. When $V_e < \eta_1$, one can conclude that the second phase of sliding surface $\boldsymbol{S}$ in (21) is asymptotically stable. Therefore, the singularity problem of terminal sliding control can be circumvented.

**Lemma 1.** *Once the ideal sliding mode motion is established, i.e., $\boldsymbol{S} = 0$, the error variables will converge to the origin within predefined time $T_1$.*

**Proof.** Consider the designed sliding manifold in (21). When $\boldsymbol{S} = 0$, it yields that

$$\boldsymbol{e}_2 = -\frac{1}{2 p_1 T_1}(1 + V_e^{p_1})^{\frac{3}{2}} V_e^{-p_1} \boldsymbol{e}_1 \tag{22}$$

Taking the time derivative of $V_e$, one has

$$\dot{V}_e = -\frac{1}{p_1 T_1}(1 + V_e^{p_1})^{\frac{3}{2}} V_e^{1-p_1} < 0 \tag{23}$$

Intuitively, the sliding mode dynamics is asymptotically stable according to the results of (23). Further, we can calculate its convergence time. Differentiating $\xi(V_e)$ with respect to time and invoking (15), one has

$$\frac{d\xi(V_e)}{dt} = \frac{d\xi}{d\left(V_e^{p_1}\right)} p_1 V_e^{p_1 - 1} \frac{dV_e}{dt} = \frac{1}{T_1} \tag{24}$$

with $\xi(V_e) = \frac{1}{\sqrt{1+V_e^{p_1}}}$ with $\xi(0) = 1$. The derivative $\dot{\xi}(V_e)$ is positive definite. Therefore, the function $\xi(V_e)$ increases to its maximum $\xi(0) = \xi_T = 1$ from its arbitrary initial value $\xi(V_{e0})$. The initial value $\xi(V_{e0}) < 1$ always holds. Integrating (24) yields

$$\int_{\xi(V_{e0})}^{\xi_T} 1 d\xi = \int_0^T \frac{1}{T_1} dt \tag{25}$$

From (25), one can obtain $T = (\xi_T - \xi(V_{e0}))T_1 < T_1$. Therefore, it is concluded that $T \leq T_1$ is valid for any initial value $\xi(V_{e0})$ increases to the maximum of $\xi(V_e)$. As a result, the Lyapunov candidate $V_e$ also converges to zero simultaneously. The selected Lyapunov candidate $V_e$ is radially unbounded. For any initial value $\boldsymbol{e}_1(0)$, it can converge to zero when $T \geq T_1$. Hence, the error variable will converge to zero along with the sliding mode surface within predefined-time $T_1$, once the ideal sliding mode is achieved. □

### 3.2. Incremental Sliding Mode Controller Design

Using the incremental attitude control system (19) and the sliding mode surface (21), one can obtain

$$\dot{\boldsymbol{S}} = \dot{\boldsymbol{x}}_{2,0} + G(\boldsymbol{x}_{2,0})\Delta\boldsymbol{\delta} + \boldsymbol{d}_1 + \frac{\boldsymbol{e}_2\Phi_1 + \boldsymbol{e}_1\dot{\Phi}_1}{2p_1T_1} - \dot{\boldsymbol{x}}_d \tag{26}$$

Then, $\dot{\Phi}$ can be computed from (21) as follows

$$\dot{\Phi}_1 = \begin{cases} (\frac{3}{2}p_1 + 1 + V_e^{-p_1})V_e^{-1}(1 + V_e^{p_1})^{\frac{1}{2}}\dot{V}_e, & V_e \geq \eta_1 \\ (\frac{3}{2}p_1 V_e^{p_1-1}(k_1V_e + k_2V_e^2) + (1 + V_e^{p_1})(k_1 + 2k_2V_e))(1 + V_e^{p_1})^{\frac{1}{2}}\dot{V}_e, & V_e < \eta_1 \end{cases} \tag{27}$$

Specifically, it can be observed that when $V_e \geq \eta_1 > 0$, $\dot{\Phi}_1$ will not exhibit singularity. When $V_e < \eta_1$, there is no negative power term of $\boldsymbol{e}_1$. Therefore, there is no singularity for the term $\dot{\Phi}$. For system (14), the incremental control input $\Delta\boldsymbol{\delta}$ is designed as

$$\Delta\boldsymbol{\delta} = G^{-1}(\boldsymbol{x}_{2,0})\big(-\dot{\boldsymbol{x}}_{2,0} + \dot{\boldsymbol{x}}_d - \frac{\boldsymbol{e}_2\Phi_1 + \boldsymbol{e}_1\dot{\Phi}_1}{2p_1T_1} - \frac{1}{2p_2T_2}(1 + V_s^{p_2})^{\frac{3}{2}}V_s^{-p_2}\boldsymbol{S} - \gamma\,\mathbf{tanh}(\frac{\boldsymbol{S}}{c})\big) \tag{28}$$

with $0 < p_2 < \frac{1}{2}$. $V_s = \frac{1}{2}\boldsymbol{S}^\top\boldsymbol{S}$ is a Lyapunov function; $T_2 > 0$ is the predefined convergence time; $\gamma$ and $c$ are positive constants. Summarizing the above analysis, the presented predefined-time sliding mode controller (28) has no singularity.

Taking the time derivative of $V_s$ and recalling (26) and (28), one has

$$\begin{aligned} \dot{V}_s &= \boldsymbol{S}^\top\left(\dot{\boldsymbol{x}}_{2,0} + G(\boldsymbol{x}_{2,0})\Delta\boldsymbol{\delta} + \boldsymbol{d}_1 + \frac{\boldsymbol{e}_2\Phi_1 + \boldsymbol{e}_1\dot{\Phi}_1}{2p_1T_1} - \dot{\boldsymbol{x}}_d\right) \\ &= \boldsymbol{S}^\top\left(-\frac{1}{2p_2T_2}(1 + bV_s^{p_2})^{\frac{3}{2}}V_s^{-p_2}\boldsymbol{S} + \boldsymbol{d}_1 - \gamma\,\mathbf{tanh}(\frac{\boldsymbol{S}}{c})\right) \\ &\leq -\frac{1}{p_2T_2}(1 + V_s^{p_2})^{\frac{3}{2}}V_s^{1-p_2} + \|\boldsymbol{d}_1\|\|\boldsymbol{S}\| - \gamma\boldsymbol{S}^\top\,\mathbf{tanh}(\frac{\boldsymbol{S}}{c}) \end{aligned} \tag{29}$$

Consider the inequality $|\chi| - \chi\tanh(\frac{\chi}{c}) \leq \bar{\eta}_0 c$ reported in [37], where $\bar{\eta}_0 = 0.2785$, $c > 0$, and $\chi \in \mathbb{R}$. Furthermore, using the fact that $\|\boldsymbol{S}\| = \sum_{i=1}^{3}(S_i^2)^{\frac{1}{2}} \leq \sum_{i=1}^{3}|S_i|$, one has

$$-\gamma\boldsymbol{S}^\top\,\mathbf{tanh}(\frac{\boldsymbol{S}}{c}) \leq \gamma\left(-\sum_{i=1}^{3}|\boldsymbol{S}_i| + 3\bar{\eta}_0 c\right) \leq -\gamma\|\boldsymbol{S}\| + \eta_2 \tag{30}$$

with $\eta_2 = 3\gamma\bar{\eta}_0 c$ being a positive constant. Then, employing Assumption 1 and (30), $\dot{V}_s$ is simplified as

$$\begin{aligned} \dot{V}_s &\leq -\frac{1}{p_2T_2}(1 + V_s^{p_2})^{\frac{3}{2}}V_s^{1-p_2} - (\gamma - \|\boldsymbol{d}_1\|)\|\boldsymbol{S}\| + \eta_2 \\ &\leq -\frac{k}{p_2T_2}(1 + V_s^{p_2})^{\frac{3}{2}}V_s^{1-p_2} + \eta_2 \\ &\leq -\frac{1}{p_2T_2}(1 + V_s^{p_2})^{\frac{3}{2}}V_s^{1-p_2} - \frac{k-1}{p_2T_2}(1 + V_s^{p_2})^{\frac{3}{2}}V_s^{1-p_2} + \eta_2 \\ &\leq -\frac{1}{p_2T_2}(1 + V_s^{p_2})^{\frac{3}{2}}V_s^{1-p_2} - \frac{k-1}{p_2T_2}V_s^{1-p_2} + \eta_2 \end{aligned} \tag{31}$$

when $-\frac{k-1}{p_2T_2}V_s^{1-p_2} + \eta_2 \leq 0$, i.e., $V_s \geq \left(\frac{\eta_2 p_2 T_2}{k-1}\right)^{\frac{1}{1-p_2}}$, the inequality (31) can be simplified as $\dot{V}_s \leq -\frac{1}{p_2T_2}(1 + V_s^{p_2})^{\frac{3}{2}}V_s^{1-p_2}$. Using the similar analytical method form (22)–(25), one can obtain that the sliding mode trajectory $\boldsymbol{S}$ thus is practical predefined-time stable and

converges to a small region $\Omega = \{\|S\| < \Omega_{sr}\}$ with its radius being $\Omega_{sr} = \left(\frac{2\eta_2 p_2 T_2}{k-1}\right)^{\frac{1}{2(1-p_2)}}$ when $t \geq T_2$.

From the previous analysis, the sliding variable $S$ will reach a small set $\Omega$ around the origin after a predefined time $T_2$. Further, the convergence region of error $\boldsymbol{e}_1$ can be determined quantificationally.

If $V_e \geq \eta_1$, one has

$$\boldsymbol{S} = \boldsymbol{e}_2 + \frac{1}{2p_1T_1}(1 + V_e^{p_1})^{\frac{3}{2}} V_e^{-p_1} \boldsymbol{e}_1 \tag{32}$$

Furthermore, one has

$$\boldsymbol{e}_2 = -\frac{1}{2p_1T_1}(1 + V_e^{p_1})^{\frac{3}{2}} V_e^{-p_1} \boldsymbol{e}_1 + \boldsymbol{\varphi} \tag{33}$$

with $\|\boldsymbol{\varphi}\| \leq \Omega_{sr}$. Differentiating $V_e$ yields

$$\begin{aligned}
\dot{V}_e &= -\frac{1}{p_1T_1}(1 + V_e^{p_1})^{\frac{3}{2}} V_e^{1-p_1} + \boldsymbol{x}_1^\top \boldsymbol{\varphi} \\
&\leq -\frac{1}{p_1T_1}(1 + V_e^{p_1})^{\frac{3}{2}} V_e^{1-p_1} + V_e + \frac{1}{2}\Omega_{sr}^2 \\
&\leq -\frac{0.5}{p_1T_1}(1 + V_e^{p_1})^{\frac{3}{2}} V_e^{1-p_1} - \frac{0.5}{p_1T_1}(1 + V_e^{p_1})^{\frac{3}{2}} V_e^{1-p_1} + V_e + \frac{1}{2}\Omega_{sr}^2 \\
&\leq -\frac{0.5}{p_1T_1}(1 + V_e^{p_1})^{\frac{3}{2}} V_e^{1-p_1} - \frac{0.5 - p_1T_1}{pT_1} V_e + \frac{1}{2}\Omega_{sr}^2
\end{aligned} \tag{34}$$

with inequality $0.5 > p_1T_1$ being met. When $-\frac{0.5-p_1T_1}{p_1T_1} V_e + \frac{1}{2}\Omega_{sr}^2 \leq 0$, i.e., $V_e \geq \frac{0.5 p_1 T_1 \Omega_{sr}^2}{0.5 - p_1T_1}$, the inequality (34) can be simplified as $\dot{V}_e \leq -\frac{0.5}{p_1T_1}(1 + V_e^{p_1})^{\frac{3}{2}} V_e^{1-p_1}$. Then, invoking the analysis process form (22)–(26), the error variable $\boldsymbol{e}_1$ will converge to a small set $\Omega_e = \left\{\lim_{t\to(T_2+2T_1)} \|\boldsymbol{e}_1\| \leq \Omega_{er}\right\}$ with its radius being $\Omega_{er} = \sqrt{\frac{p_1 T_1 \Omega_{sr}^2}{0.5 - p_1T_1}}$ in predefined time.

For the case $V_e < \eta_1$, the error variable $\boldsymbol{e}_1$ converges to the region $\bar{\Omega}_e = \{\|\boldsymbol{e}_1\| \leq \max\{\sqrt{2\eta_1}, D_3\}\}$. Consequently, one can conclude that $\boldsymbol{e}_1$ will converge to the region $\Omega_e$ within predefined time $t \leq 2T_1 + T_2$. Therefore, the predefined-time stability of the attitude control system can be guaranteed under the action of the proposed controller (28). Summarizing the above results, we can derive the following theorem.

**Theorem 1.** *In view of the attitude control system* (17) *with Assumption* 1*, let the predefined-time incremental sliding mode control law be designed as* (28)*. The system closed-loop with the control input* $\boldsymbol{\delta} = \boldsymbol{\delta}_0 + \Delta\boldsymbol{\delta}$ *is practical predefined time stable even under external disturbances and uncertainties.*

To obtain a better tracking control performance, the following procedures can be used to select the control gains for Theorem 1.

*Step 1:* Set an attitude convergence time upper bound $T_s$ such that $T_s = T_1 + T_2$ based on the actual tracking task requirements;

*Step 2:* Choose a positive constant $\gamma$ such that Assumption 1;

*Step 3:* Select positive constants $p_i$ ($i$ = 1, 2) such that $0 < p_i < 0.5$ and $p_1T_1 < 0.5$;

*Step 4:* Select a small enough positive constant $\eta_1$, which can adjust the convergence accuracy of attitude tracking error, and the smaller its value, the higher the convergence accuracy.

Following the aforementioned steps, and then examining whether the tasks' corresponding tracking performance is desired or not. If not, then repeat Steps 3 and 4 to rechoose the gains $p_i$ and $\eta_1$ until the desired performance is achieved.

It should be pointed out that as the predefined time parameters $T_s$ decrease, the maximum torque of the controller will increase, and the control accuracy can be further

improved. Therefore, users need to balance convergence time, control torque, and control accuracy when setting predefined convergence times.

## 4. Simulation Results

To complete attitude maneuver missions, this section employs two numerical simulation examples to verify the high-precision, predefined-time attitude tracking for the eVTOL vehicle in both helicopter and airplane modes by using the incremental sliding mode control scheme $\boldsymbol{\delta} = \boldsymbol{\delta}_0 + \Delta\boldsymbol{\delta}$ (denoted as ISMC). In simulation, the sampling period is set as $\lambda = 0.01$. For the purpose of comparison, a traditional incremental dynamic inversion (denoted as INDI) method in [25] is adopted in this section to conduct comparative simulations. The lumped external disturbances in the numerical simulation are assumed as

$$\boldsymbol{d}_\omega = \begin{bmatrix} 1.2\cos(5\varrho t) + 5.8\sin(3\varrho t) - 20 \\ 2.2\cos(5\varrho t) + 6.1\sin(3\varrho t) + 25 \\ -3.8\cos(5\varrho t) - 7.2\sin(3\varrho t) + 30 \end{bmatrix} \times 10^{-2}\ \text{Nm} \tag{35}$$

with $\varrho = ||\boldsymbol{e}_2|| + 0.001$. The initial settings of the eVTOL vehicle attitude control system are given as $\boldsymbol{\Theta}(0) = [-1\ \ 0.5\ \ 0.2]^{\mathrm{T}}$ deg and $\boldsymbol{\omega}(0) = [0\ \ 0\ \ 0]^{\mathrm{T}}$deg/s. Each flight mode has different attitude commands, which will be provided later. The main control gains in (28) are selected as $p_1 = 0.02$, $p_2 = 0.01$, $T_1 = 5$, and $T_2 = 5$.

### *4.1. Attitude Tracking Control in Helicopter Mode*

For the helicopter mode of the target eVTOL vehicle, the scenario considered is to adjust the attitude of the eVTOL vehicle to complete low-speed acceleration when it is in hover. Provide the desired commands for the eVTOL vehicle attitude control system's pitch angle, roll angle, and yaw angle; that is, first roll the vehicle to the right by 5 degrees, then pitch it forward by 5 degrees, and finally change the heading by 10 degrees. Finally, all the attitude angles will return to 0 degrees and remain stable. The performance of attitude tracking control in helicopter mode is verified through control methods INDI and ISMC. The comparative simulation results are shown in Figures 2–4. It is obvious that the suggested ISMC controller $\boldsymbol{\delta}$ is defined in Theorem 1 can enforce the attitude control system quickly following the command attitude signals with an overshoot of less than 2%. The control method INDI can also drive the attitude control system to track the desired command, but it has a lower response speed and a larger tracking error.

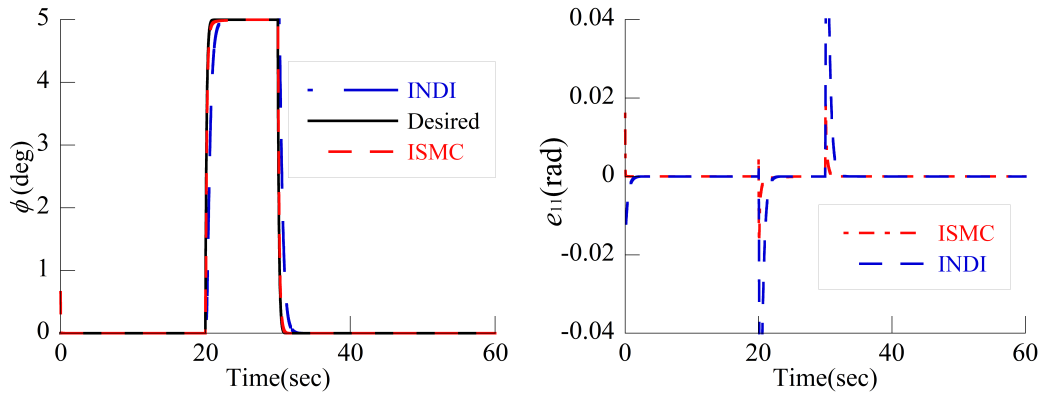



**Figure 2.** Attitude tracking performance in helicopter mode: (**a**) The tracking performance of roll angle; (**b**) The tracking error of roll angle.

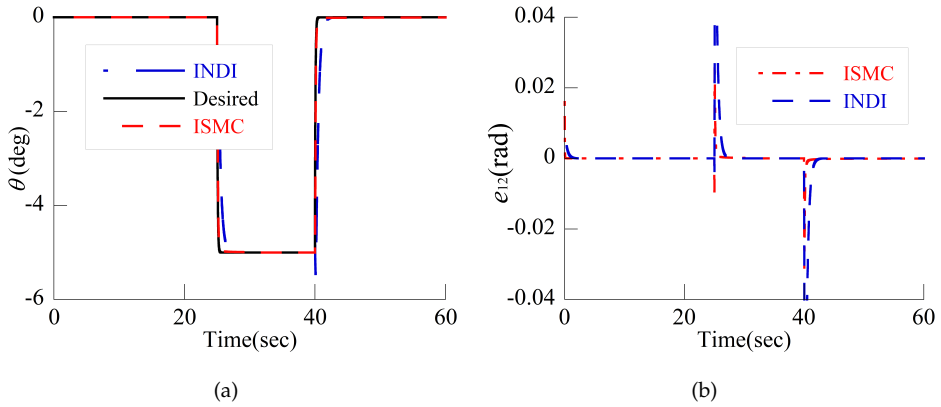



**Figure 3.** Attitude tracking performance in helicopter mode: (**a**) The tracking performance of pitch angle; (**b**) The tracking error of pitch angle.

As shown in Figures 2b, 3b and 4b, the tracking error of the three attitude angles remains under ISMC within a small region around zero; that is to say, the corresponding tracing errors satisfy $|\phi - \phi_d| \leq 0.02$ rad, $|\theta - \theta_d| \leq 0.02$ rad, and $|\psi - \psi_d| \leq 0.01$ rad. Compared with the INDI method, the tracking error of the attitude control system under the ISMC method is smaller. Moreover, the convergence time of the error meets the parameter setting of the predefined time, that is, $t < 2T_1 + T_2 = 15$ s. It is observed that the introduced disturbances have little effect on the actual response, as shown in Figures 2a, 3a, and 4a. Finally, the given incremental controller $\delta$ calculates the required moment that each control channel needs to provide, shown in Figure 5. It can be observed that at the 20th, 25th, and 40th s, there are large peaks in the moment required for each decoupling channel. This is due to the expected command undergoing a step change at these time points, which poses a significant challenge to the rapid response of the eVTOL vehicle's attitude control system. According to Figure 5, the ISMC method requires a larger control torque for the attitude control system compared with the INDI method. This is because for converging the attitude within a predefined time with faster response and higher convergence accuracy, a larger torque needs to be provided. Figures 2–4 also confirm these conclusions. It should be noted that achieving a fast response requires a large instantaneous torque. In practical applications, it is necessary to balance the system's fast stability with its actual control energy efficiency. This can be achieved by adjusting the controller parameters to achieve better control performance.

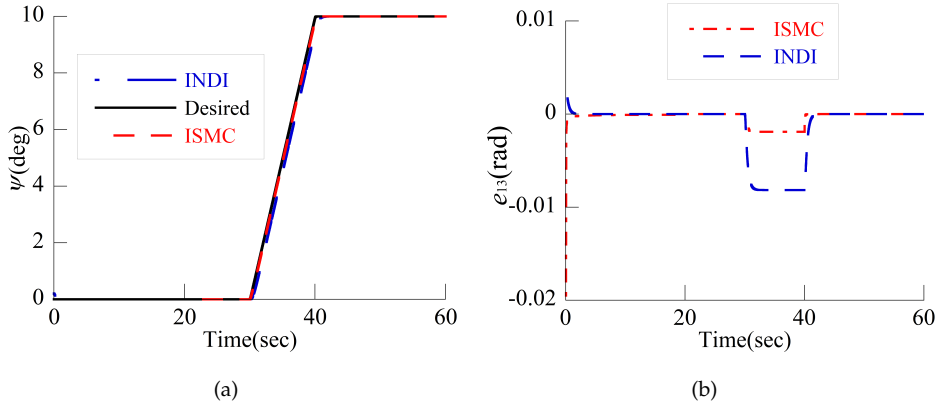



**Figure 4.** Attitude tracking performance in helicopter mode: (**a**) The tracking performance of yaw angle; (**b**) The tracking error of yaw angle.

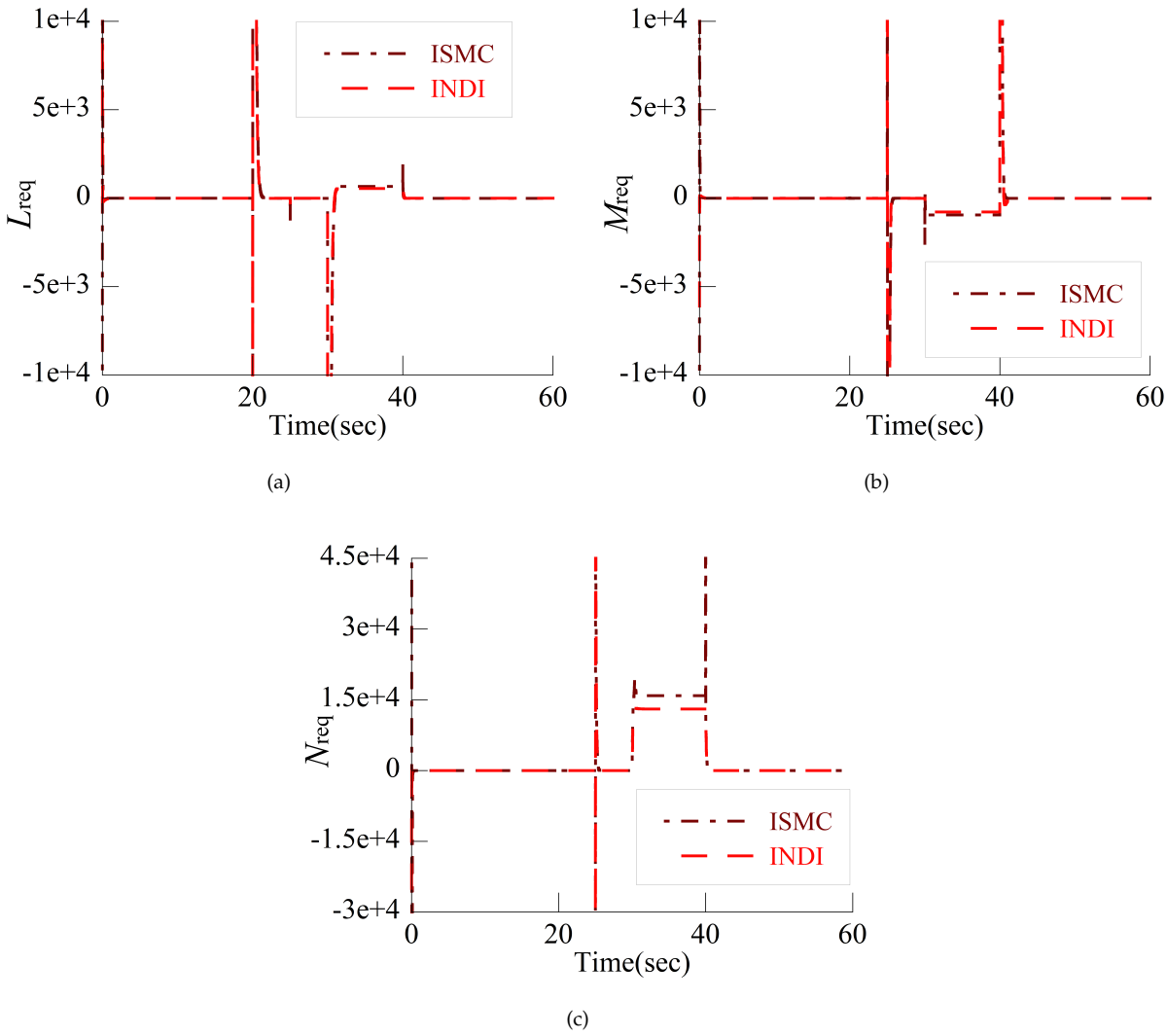
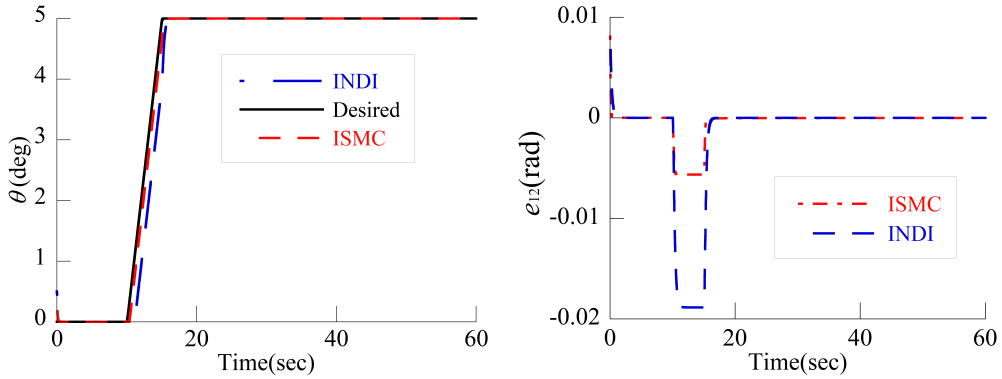



**Figure 5.** Required moments by rotors in helicopter mode: (**a**) The roll angle control channel; (**b**) The pitch angle control channel; (**c**) The yaw angle control channel.

### *4.2. Attitude Tracking Control in Airplane Mode*

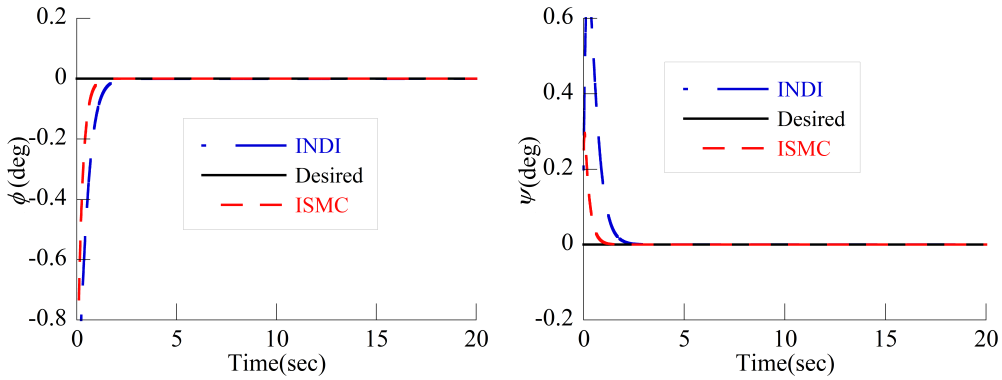
We continue to investigate the control performance of the control methods ISMC and INDI applied to the airplane mode of the target eVTOL vehicle. The scenario considered is to adjust the attitude of the vehicle to complete a cruise maneuver mission. In this case, the vehicle needs to complete a 10-degree pitch attitude maneuver while cruising, while keeping the yaw and roll angles unchanged at 0 degrees. The performance of attitude tracking control in airplane mode is verified through numerical simulation, and the comparative simulation results are shown in Figures 6 and 7. It is obvious that the suggested ISMC scheme $\delta$ defined in Theorem 1 can drive the attitude control system to quickly follow the command attitude signals with an overshoot of less than 1%. As shown in Figures 6b and 7, the tracking error of the three attitude angles remains within a small region around zero; that is to say, the corresponding tracing errors satisfy $|\phi - \phi_d| \leq 0.8$ deg, $|\theta - \theta_d| \leq 0.29$ deg, and $|\psi - \psi_d| \leq 0.4$ deg. Compared with the comparative INDI method, the tracking accuracy of the control system with the ISMC method is smaller. Moreover, the convergence time of the error meets the parameter setting of the predefined time, that is, $t < 2T_1 + T_2 = 15$ seconds. It is observed that the introduced disturbances have little effect on the actual response, as shown in Figures 6a and 7. Finally, the given ISMC scheme $\delta$ calculates the required moment that each control channel must provide,

shown in Figure 8. Moreover, Figure 8b gives the required control torque for the pitch control channel of the eVTOL vehicle, which needs to be kept constant so that the vehicle can complete the pitch maneuver of the attitude between 15 s and 20 s.




(a) (b)

**Figure 6.** Attitude tracking performance in airplane mode: (**a**) The tracking performance of pitch angle; (**b**) The tracking error of pitch angle.




(a) (b)

**Figure 7.** Attitude tracking performance in airplane mode: (**a**) The tracking performance of roll angle; (**b**) The tracking performance of yaw angle.

### *4.3. Discussion*

This paper proposes a new predefined-time incremental sliding mode control scheme to achieve attitude tracking of an eVTOL. Compared with these sliding mode control methods in [38–42], the incremental sliding mode control scheme designed in this paper has lower dependence on the model and has better engineering application prospects. Compared with the incremental control scheme [2,22,24], this paper retains the high-order terms of Taylor expansion instead of directly discarding them, thus increasing the modeling accuracy of the attitude augmentation model. However, the limitation of this paper is that it does not take into account the need for large instantaneous torque while achieving predefined-time convergence through the given predefined time controller. This could lead to an actuator saturation problem. It is critical to balance the system's rapid stability with its actual actuator constraint.

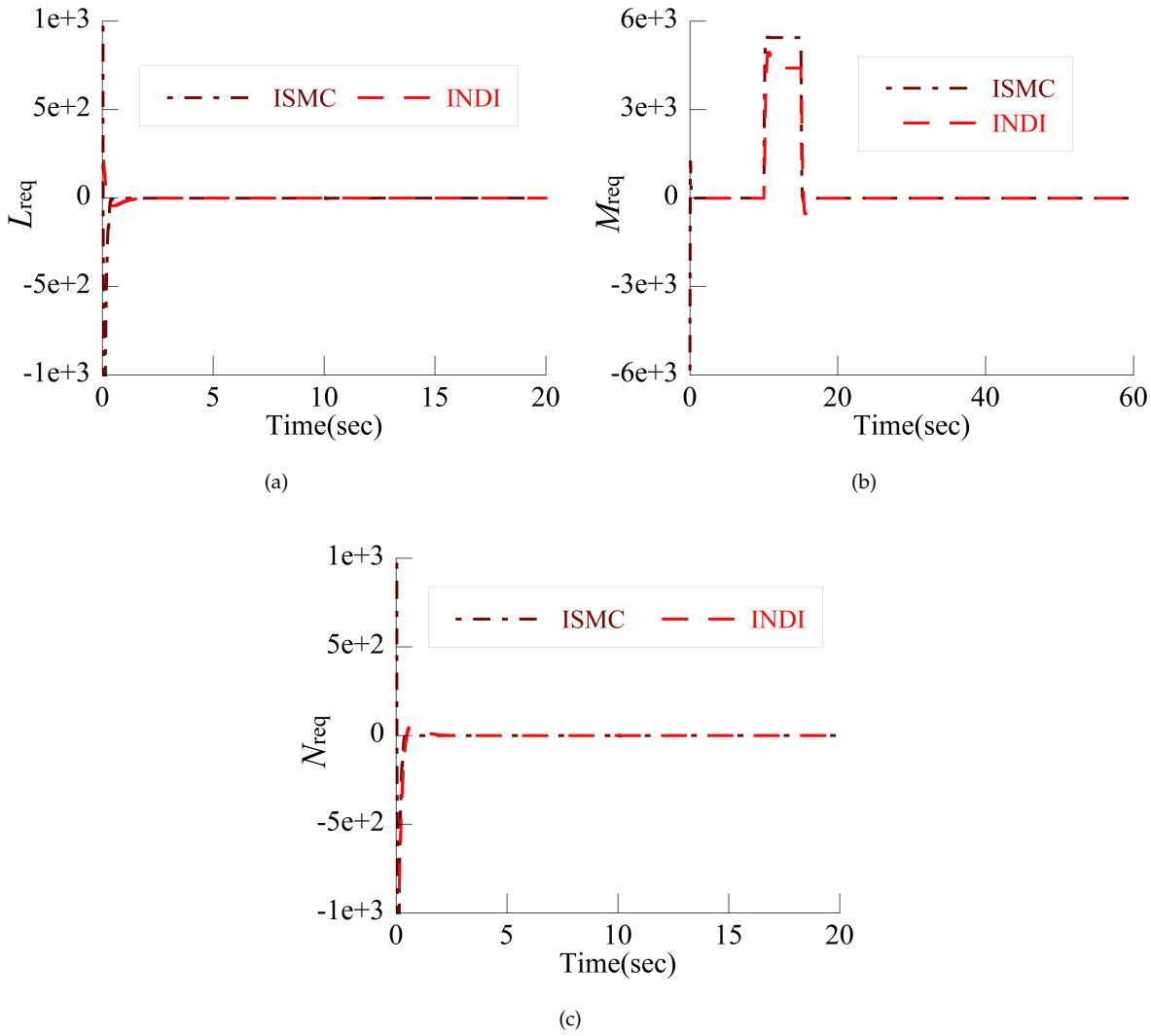



**Figure 8.** Required moments by control effectors in airplane mode: (**a**) The roll angle control channel; (**b**) The pitch angle control channel; (**c**) The yaw angle control channel.

## 5. Conclusions

This paper proposes a low-model dependency attitude control solution for an eVTOL vehicle's attitude tracking control problem in helicopter mode and airplane mode. It not only ensures the predefined-time stability of the controlled system but also guarantees the strong robustness of the whole controlled system. The first step involves establishing an incremental model for the eVTOL vehicle attitude control system that incorporates external disturbances. Compared with existing incremental control methods that directly ignore high-order terms in the Taylor expansion process, this paper preserves high-order terms and instantaneous perturbations as a lumped term, enhancing the accuracy of the incremental model. A predefined-time incremental control solution based on the designed sliding surface and incremental control methods is proposed, which also synthesizes robust control commands. It effectively reduces reliance on model information and attenuates the impact of external disturbances. The proposed control solution is better than existing asymptotically stable and finite-time stable incremental control solutions because it can set the convergent time upper bound of the controlled system ahead of time. The simulation results also support this conclusion. However, from a theoretical perspective, predefined time control methods often lead to actuator saturation when the time constant is too small. Future research needs to address this issue. From an engineering perspective, future

research needs to establish a hardware-in-the-loop experimental platform to verify the control performance under system uncertainties of the designed control scheme in practical applications, including measurement noise, actuator installation deviation, and so on.

**Author Contributions:** Conceptualization, J.L. and Y.T.; methodology, J.L. and Y.T.; software, J.L.; validation, J.L. and Y.T.; investigation, J.L.; resources, J.L. and Y.T.; writing—original draft preparation, J.L.; writing—review and editing, J.L. and Y.T.; supervision, Y.T. All authors have read and agreed to the published version of the manuscript.

**Funding:** This research was funded by National Natural Science Foundation of China (U19A2060) and Guangzhou Government-University (Hospital)-Enterprise joint funding project (2023A03J0126).

**Data Availability Statement:** Datasets available upon request from the authors.

**Acknowledgments:** The authors sincerely appreciate to the editors' and reviewers' kind attention and valuable comments dedicated to this paper.

**Conflicts of Interest:** The authors declare no conflicts of interest.. Jujiang Liu was employed by the Guangzhou Automobile Group Co., Ltd.. The remaining author declare that the research was conducted in the absence of any commercial or financial relationships that could be construed as a potential conflict of interest.

## References

1. Xiang, S.; Xie, A.; Ye, M.; Yan, X.; Han, X.; Niu, H.; Li, Q.; Huang, H. Autonomous eVTOL: A summary of researches and challenges. *Green Energy Intell. Transp.* **2024**, *3*, 100140.
2. Ye, Z.; Chen, Y.; Cai, P.; Lyu, H.; Gong, Z.; Wu, J. Control design for soft transition for landing preparation of light compound-wing unmanned aerial vehicles based on incremental nonlinear dynamic inversion. *Appl. Sci.* **2023**, *13*, 12225. [CrossRef]
3. Liu, Z.; He, Y.; Yang, L.; Han, J. Control techniques of tilt rotor unmanned aerial vehicle systems: A review. *Chin. J. Aeronaut.* **2017**, *30*, 135–148. [CrossRef]
4. Wang, M.; Chu, N.; Bhardwaj, P.; Zhang, S.; Holzapfel, F. Minimum-time trajectory generation of eVTOL in low-speed phase: Application in control law design. *IEEE Trans. Aerosp. Electron. Syst.* **2023**, *59*, 1260–1275. [CrossRef]
5. Qiao, Z.; Wang, D.; Xu, J.; Pei, X.; Su, W.; Wang, D.; Bai, Y. A comprehensive design and experiment of a biplane quadrotor tail-sitter UAV. *Drones* **2023**, *7*, 292. [CrossRef]
6. Rohr, D.; Stastny, T.; Verling, S.; Siegwart, R. Attitude and cruise control of a VTOL tiltwing UAV. *IEEE Robot. Autom. Lett.* **2019**, *4*, 2683–2690. [CrossRef]
7. Mao, S.; Gong, Z.; Ye, Z.; Wang, Z.; Guo, T.; Zhang, C. A linear-active-disturbance-rejection-based vertical takeoff and acceleration strategy with simplified vehicle operations for electric vertical takeoff and landing vehicles. *Mathematics* **2022**, *10*, 3333. [CrossRef]
8. Deng, Z.; Wu, L.; You, Y. Modeling and design of an aircraft-mode controller for a fixed-wing VTOL UAV. *Math. Probl. Eng.* **2021**, *2021*, 7902134. [CrossRef]
9. Allenspach, M.; Ducard, G.J.J. Nonlinear model predictive control and guidance for a propeller-tilting hybrid unmanned air vehicle. *Automatica* **2021**, *132*, 109790. [CrossRef]
10. Xili, Y.; Yong, F.; Jihong, Z. Transition flight control of two vertical/short takeoff and landing aircraft. *J. Guid. Control Dyn.* **2008**, *31*, 371–385.
11. Ajel, A.R.; Humaidi, A.J.; Ibraheem, I.K.; Azar, A.T. Robust model reference adaptive control for tail-sitter VTOL aircraft. *Actuators* **2021**, *10*, 162. [CrossRef]
12. Liu, N.; Cai, Z.; Wang, Y.; Zhao, J. Fast level-flight to hover mode transition and altitude control in tiltrotor's landing operation. *Chin. J. Aeronaut.* **2021**, *34*, 181–193. [CrossRef]
13. Liang, Z.; Fan, L.; Wen, G.; Xu, Z. Design, modeling, and control of a composite tilt-rotor unmanned aerial vehicle. *Drones* **2024**, *8*, 102. [CrossRef]
14. Dalwadi, N.; Deb, D.; Kothari, M.; Ozana, S. Disturbance Observer-Based Backstepping Control of Tail-Sitter UAVs. *Actuators* **2021**, *10*, 119. [CrossRef]
15. Yang, H.; Morales, R. Robust full-envelope flight control design for an evtol vehicle. In Proceedings of the AIAA Scitech 2021 Forum, Online, 19–21 January 2021; p. 0254.
16. Yun, W.J.; Jung, S.; Kim, J.; Kim, J.H. Distributed deep reinforcement learning for autonomous aerial eVTOL mobility in drone taxi applications. *ICT Express* **2021**, *7*, 1–4. [CrossRef]
17. Lane, S.; Stengel, R. Flight control design using non-linear inverse dynamics. *Automatica* **1988**, *24*, 471–483. [CrossRef]
18. Georgie, J.; Valasek, J. Evaluation of longitudinal desired dynamics for dynamic-inversion controlled generic reentry vehicles. *J. Guid. Control Dyn.* **2003**, *26*, 811–819. [CrossRef]
19. Enenakpogbe, E.; Whidborne, J.F.; Lu, L. Control of an eVTOL using non-linear dynamic inversion. In Proceedings of the 2022 UKACC 13th International Conference on Control, Plymouth, UK, 20–22 April 2022; pp. 158–164.

20. Lombaerts, T.; Kaneshige, J.; Schuet, S.; Hardy, G.; Aponso, B.; Shish, K. Dynamic inversion based full envelope flight control for an eVTOL vehicle using a unified framework. In Proceedings of the AIAA Scitech 2020 Forum, Orlando, FL, USA, 6–10 January 2020; p. 1619.
21. Sieberling, S.; Chu, Q.P.; Mulder, J.A. Robust flight control using incremental nonlinear dynamic inversion and angular acceleration prediction. *J. Guid. Control Dyn.* **2010**, *33*, 1732–1742. [CrossRef]
22. Wang, X.; van Kampen, E.J.; Chu, Q.; Lu, P. Stability analysis for incremental nonlinear dynamic inversion control. *J. Guid. Control Dyn.* **2019**, *42*, 1116–1129. [CrossRef]
23. Sun, S.; Wang, X.; Chu, Q.; de Visser, C. Incremental nonlinear fault-tolerant control of a quadrotor with complete loss of two opposing rotors. *IEEE Trans. Robot.* **2021**, *37*, 116–130. [CrossRef]
24. Di Francesco, G.; Mattei, M. Modeling and incremental nonlinear dynamic inversion control of a novel unmanned tiltrotor. *J. Aircr.* **2016**, *53*, 73–86. [CrossRef]
25. Lombaerts, T.; Kaneshige, J.; Schuet, S.; Hardy, G.; Aponso, B.; Shish, K. Nonlinear dynamic inversion based attitude control for a hovering quad tiltrotor evtol vehicle. In Proceedings of the AIAA Scitech 2019 Forum, San Diego, CA, USA, 7–11 January 2019; p. 0134.
26. Suiçmez, E.; Kutay, A. Full envelope nonlinear flight controller design for a novel electric VTOL (eVTOL) air taxi. *Aeronaut. J.* **2024**, *128*, 966–993. [CrossRef]
27. Matamoros, I.; de Vissery, C. Incremental nonlinear control allocation for a tailless aircraft with innovative control effectors. In Proceedings of the AIAA Guidance, Navigation, and Control Conference, Honolulu, HI, USA, 18–21 August 2018; p. 1116.
28. Wang, X.; Sun, S. Incremental fault-tolerant control for a hybrid quad-plane UAV subjected to a complete rotor loss. *Aerosp. Sci. Technol.* **2022**, *125*, 107105. [CrossRef]
29. Zhang, S.; Han, W.; Zhang, Y. Finite time convergence incremental nonlinear dynamic inversion-based attitude control for flying-wing aircraft with actuator faults. *Actuators* **2020**, *9*, 70. [CrossRef]
30. Liu, J.; Sun, L.; Tan, W.; Liu, X.; Li, G. Finite time observer based incremental nonlinear fault-tolerant flight control. *Aerosp. Sci. Technol.* **2020**, *104*, 105986. [CrossRef]
31. Tal, E.; Karaman, S. Accurate tracking of aggressive quadrotor trajectories using incremental nonlinear dynamic inversion and differential flatness. *IEEE Trans. Control Syst. Technol.* **2021**, *29*, 1203–1218. [CrossRef]
32. Zhou, Y.; Van Kampen, E.J.; Chu, Q. Incremental approximate dynamic programming for nonlinear adaptive tracking control with partial observability. *J. Guid. Control Dyn.* **2018**, *41*, 2554–2567. [CrossRef]
33. Zhou, Y.; van Kampen, E.J.; Chu, Q.P. Incremental model based online dual heuristic programming for nonlinear adaptive control. *Control Eng. Pract.* **2018**, *73*, 13–25. [CrossRef]
34. Acquatella, B.P.; Chu, Q.P. Agile spacecraft attitude control: An incremental nonlinear dynamic inversion approach. *IFAC-PapersOnLine* **2020**, *53*, 5709–5716. [CrossRef]
35. Meng, Q.; Yang, H.; Jiang, B. Fault-tolerant optimal spacecraft attitude maneuver: An incremental model approach. *J. Guid. Control Dyn.* **2022**, *45*, 1676–1691. [CrossRef]
36. Bacon, B.; Ostroff, A.; Joshi, S. Reconfigurable NDI controller using inertial sensor failure detection & isolation. *IEEE Trans. Aerosp. Electron. Syst.* **2001**, *37*, 1373–1383.
37. Xiao, B.; Zhang, H.; Chen, Z.; Cao, L. Fixed-time fault-tolerant optimal attitude control of spacecraft with performance constraint via reinforcement learning. *IEEE Trans. Aerosp. Electron. Syst.* **2023**, *59*, 7715–7724. [CrossRef]
38. Moulay, E.; Léchappé, V.; Bernuau, E.; Defoort, M.; Plestan, F. Fixed-time sliding mode control with mismatched disturbances. *Automatica* **2022**, *136*, 110009. [CrossRef]
39. Xiao, B.; Zhang, H.; Zhao, S.; Chen, Z.; Cao, L. Unified sufficient conditions for predefined-time stability of non-linear systems and its standard controller design. *Actuators* **2024**, *13*, 173. [CrossRef]
40. Feng, Y.; Yu, X.; Han, F. On nonsingular terminal sliding-mode control of nonlinear systems. *Automatica* **2013**, *49*, 1715–1722. [CrossRef]
41. Wu, C.; Yan, J.; Shen, J.; Wu, X.; Xiao, B. Predefined-time attitude stabilization of receiver aircraft in aerial refueling. *IEEE Transactions on Circuits and Systems II: Express Briefs* **2021**, *68*, 3321–3325. [CrossRef]
42. Zhang, H.; Chen, Z.; Xiao, B.; Li, B. Fast fixed-time attitude tracking control of spacecraft with prescribed performance. *Int. J. Robust Nonlinear Control* **2023**, *33*, 5229–5245. [CrossRef]


**Disclaimer/Publisher's Note:** The statements, opinions and data contained in all publications are solely those of the individual author(s) and contributor(s) and not of MDPI and/or the editor(s). MDPI and/or the editor(s) disclaim responsibility for any injury to people or property resulting from any ideas, methods, instructions or products referred to in the content.